Lateral Torsional Buckling of Steel Bridge Girders

Raphaël Thiébaud[1], Jean-Paul Lebet[2], André Beyer[3], Nicolas Boissonnade[4]

Abstract

The Lateral Torsional Buckling (L.T.B.) design of beams in buildings has received considerable attention over the last decades, and relatively similar improved design rules are now implemented in major design standards. On the contrary, it may be shown that the various available design specifications for the L.T.B. design check of bridge girders still lead to significant discrepancies regarding the reduction curve to be used. Furthermore, the resistance to L.T.B. of steel bridges depends on several specific parameters such as cross-bracings, geometric imperfections and residual stresses. The present paper investigates both experimentally and numerically the influence of these parameters on the resistance to L.T.B., and proposes improved design rules.

1. Introduction

Lateral torsional buckling (L.T.B.) is a complex instability phenomenon which occurs when a girder is bent about its major-axis. Numerous experimental and theoretical studies have already been conducted to evaluate the resistance of steel girders – building-type girders mainly. The obtained results have been used as the basis for current steel construction standards. In the field of steel and composite bridge girders, few experimental and theoretical studies exist in order to evaluate their structural security particularly with respect to L.T.B.

Within steel bridges, L.T.B. may occur at various stages in the life of the structure, from erection/deconstruction (Figs. 1a, 1b and 2b), to launching and service life (Figs. 1c and 2a). Also, composite bridges made of several parallel girders (Fig. 2b) require adequate and careful design of lateral braces for the erection phases, so as to limit unbraced lengths of the girders prone to L.T.B.

Moreover, steel bridge girders are typically fabricated with thin, slender plates. These girders usually exhibit a full three dimensional response, and are influenced by a number of key parameters including cross-bracing, variable geometry of cross-sections, local buckling owing to slender webs, loading distributions or even aspects related to manufacturing and to material behavior. Typically, the manufacturing of such girders consists in flame cutting the flanges

---

[1] PhD, École Polytechnique Fédérale de Lausanne, <raph.thiebaud@gmail.com>
[2] Professor, École Polytechnique Fédérale de Lausanne, <jean-paul.lebet@epfl.ch>
[3] Graduate Student, CTICM, <aBeyer@cticm.com>
[4] Professor, University of Applied Sciences of Western Switzerland, <nicolas.boissonnade@hefr.ch>

followed by welding a thin web to the thick flanges – with or without longitudinal stiffeners in the web. This results in specific geometrical imperfections on the constituent plates as well as in particular residual stresses whose influence on the behavior of the structure is not to be neglected. Consequently, beyond being complex, the L.T.B. behavior of bridge girders deserves specific attention and shall in particular be differentiated from that of building beams.
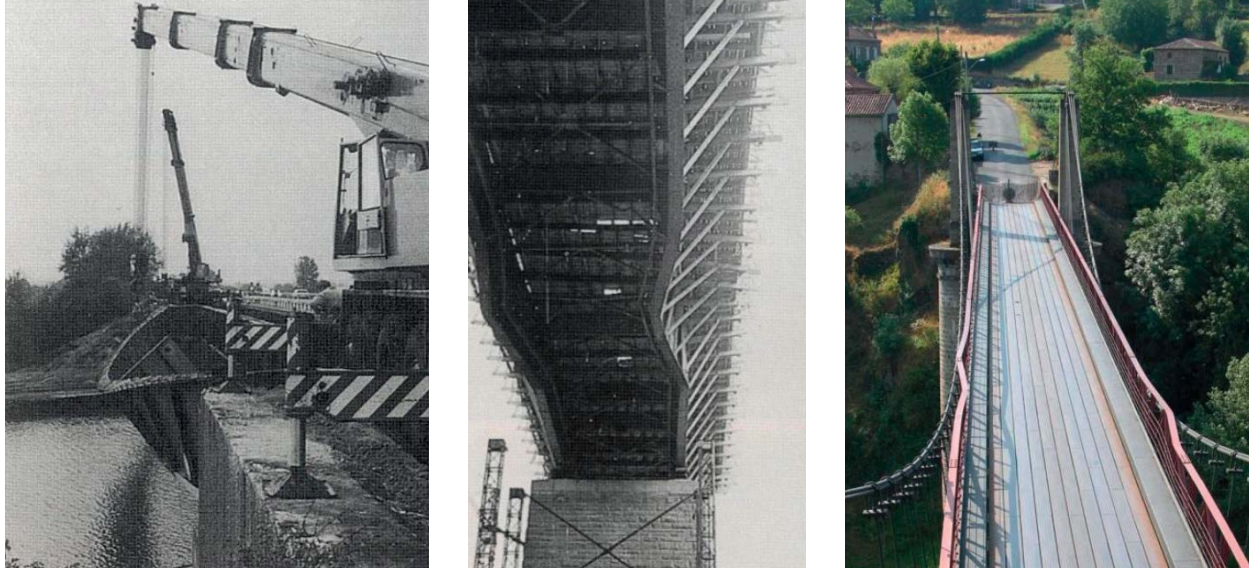

Figure 1: Lateral Torsional Buckling of steel bridges. (a) During deconstruction. (b) During erection (concreting phase), lower flange (hogging moment). (c) In service, upper flange (sagging moment)
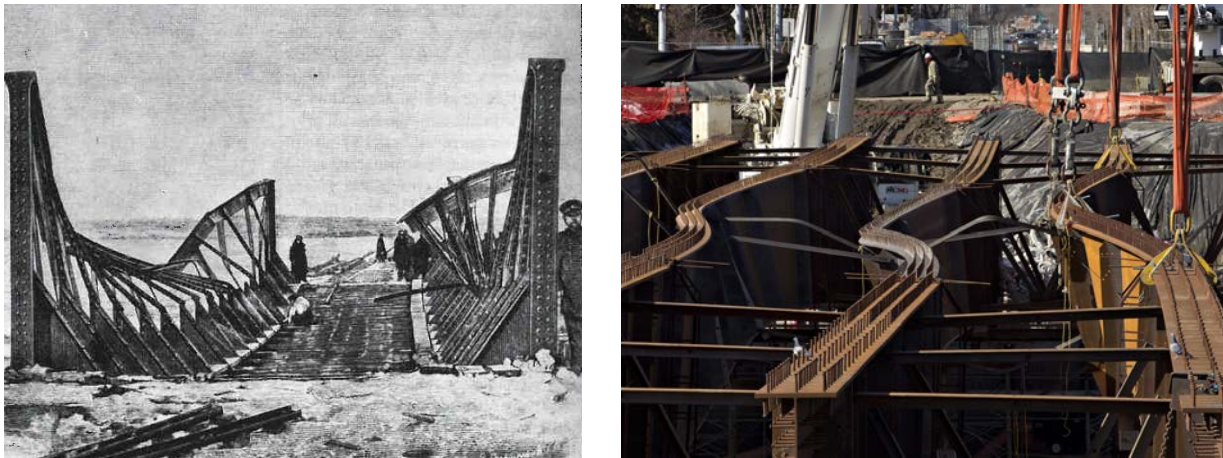

Figure 2: Lack of horizontal bracing in steel bridges. (a) In service. (b) During construction

This paper presents the results of experimental and theoretical research works towards the L.T.B. of steel bridge girders. It first focuses on the determination of suitable residual stresses patterns (Section 2) that shall be recommended in numerical Finite Element (F.E.) studies, as based on experimental measurements. Then, Section 3 exposes the L.T.B. design recommendations used in Europe for bridge girders, and presents numerical models used to characterize the L.T.B. response of steel bridges in the present study. F.E. numerical studies covering the various influences of residual stresses, geometrical imperfections and cross-bracings are detailed in Section 4. Last, Section 5 analyses the numerical results as compared to design recommendations, and proposes a L.T.B. verification suited to steel bridge girders.

2. Residual stresses in welded (bridge) sections

2.1. Typical residual stresses patterns

Typical residual stresses models for bridge welded sections can be divided in two groups: models corresponding to *flame-cut* plates (mostly thick flanges), and models corresponding to *rolled* flanges. The models for flame-cut plates (Fig. 3) are characterized by tension blocks in the flanges' edges and in the vicinity of the welds, and by compression blocks in the transition zones. Widths of tensile and compressive zones as well as the corresponding residual stresses are different in the two models. In particular, the model exposed in Fig. 3a shows tensile residual stresses at the edges equal to the yield stress f_y. Note that this model is plate-by-plate self-equilibrated.
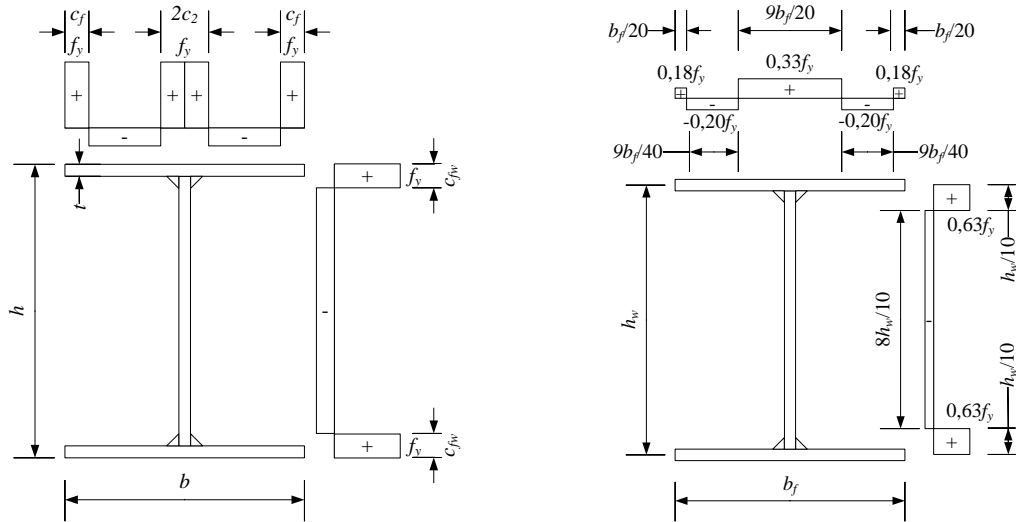

Figure 3: Residual stresses distributions for welded profiles with flame-cut plates. (a) Welded profile according to E.C.C.S. (ECCS, 1976). (b) Welded profile according to Chacon et al. (Chacon, 2009)

Others authors have proposed variants to this model as illustrated in Fig. 3b. The latter is a simplified version of Fig. 3a model for numerical simulation purposes. It differs firstly by the tensile and compressive widths which are function of the flange width b_f and the web height h_w. Secondly, it shows lower values of tensile and compressive residual stresses. This model is no more plate-by-plate self-equilibrated.

Examples of models for residual stresses in welded profiles with rolled plates are presented in Fig. 4. The distribution is characterized by tensile stresses at the weld zone equilibrated by compressive stresses on the remaining zones. The first such model found in the literature (Fig. 4a) proposes a stress value equal to f_y for the welded zone with a linear transition to the compressive zone where the residual stress is equal to $-0.25 f_y$. The tensile and compressive widths are function of plate's geometries. The other model (Fig. 4b) differs from the previous one with a direct transition between the tensile and compressive zones and with block widths that are mainly a function of plates' thickness. This latter model can as well be shown to be plate-by-plate self-equilibrated.
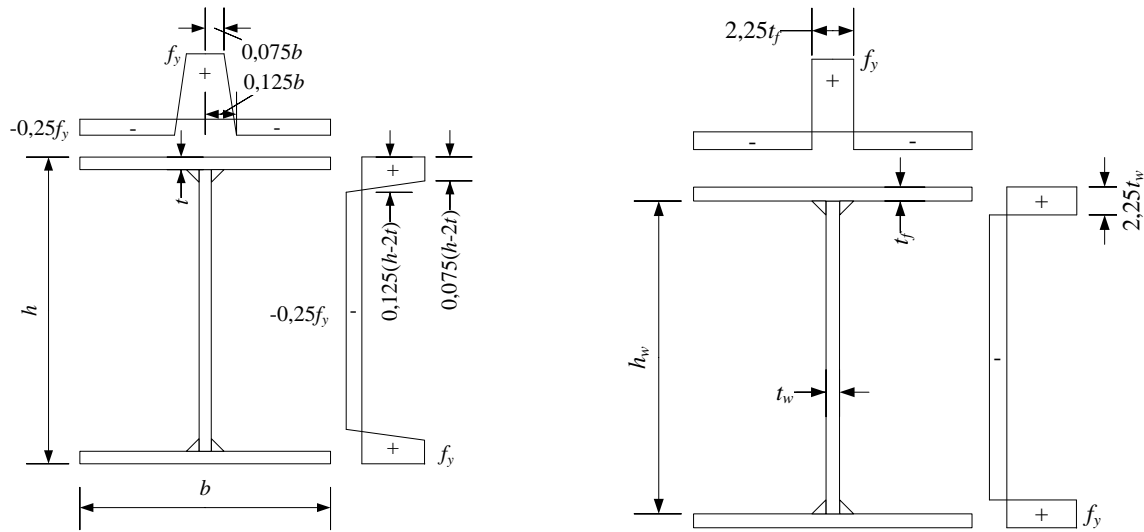
Figure 4: Residual stresses distributions for welded profiles with rolled plates. (a) Welded profile with $f_y = 235$ *MPa* according to E.C.C.S. (ECCS, 1984). (b) Welded profile according to Gozzi et al. (Gozzi, 2007).

2.2. Measurements of residual stresses in welded plates

In order to define a more adequate residual stresses model for steel bridge girders, experimental activities were conducted at the Steel Structures Laboratory (ICOM) of the Ecole Polytechnique Fédérale de Lausanne (Lausanne, Switzerland). Indeed, very few models take into consideration all the phases of steel bridge girders manufacturing, that is flat rolling, flame cutting of thick flanges and web-flange welding.
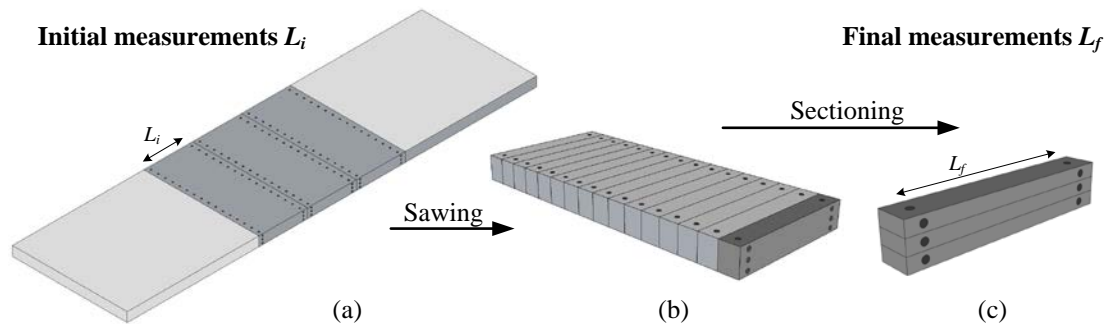

Figure 5: Principles of the sectioning method

Dedicated residual stresses measurements were done using the sectioning method (Fig. 5, Tebedge, 1973). They were performed on different S355 steel plates corresponding to the flanges of flame-cut girders and flame-cut girders with a welded web (Fig. 6). The flange plates were 60 *mm* thick and between 615 and 730 *mm* wide. The web plate was 20 *mm* thick (Fig. 6).

The results of the residual stresses measurements are presented in Fig. 7 for flame-cut and welded specimens.
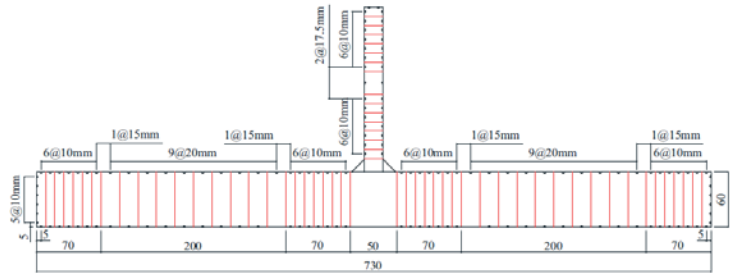
Figure 6: Experimental division of flange into strips (flame-cut specimen with width of 730 *mm*)

Fig. 7a shows that flame cutting locally introduces a high residual tensile stress on the flange's edges reaching approximately 250 *MPa*. This tension part is followed by a compressive zone, and the influence of welding is seen to be the introduction of further tensile stresses in the thermally-affected area near the welds, reaching about 50 *MPa* at peak. By dividing the edge distance by the sample width b_f and the residual stresses by the yield stress f_y, the results can be translated into a non-dimensional pattern, as represented in Fig. 7b. This model has served as a basis for the numerical simulations in this study.
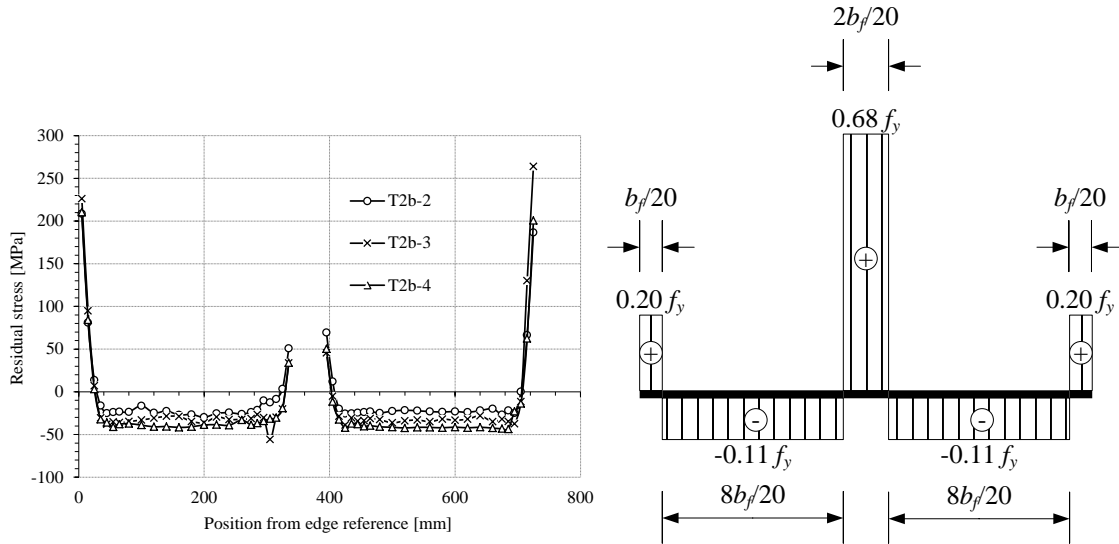

Figure 7: Flame-cut flanges. (a) Distribution of the average residual stresses measured for welded samples. (b) Non-dimensional residual stresses experimental model proposed

3. Lateral Torsional Buckling checks – F.E. parametric studies

3.1. Design according to Eurocodes/Swiss standards

Eurocode 3 Part 2 (bridges) EN1993-2:2006 (CEN, 20016) proposes two verification methods for the lateral buckling of beams in its clause 6.3.4: a general method (§ 6.3.4.1) and a simplified one (§ 6.3.4.2). These approaches differ in the calculation of the so-called relative slenderness λ_{LT} but are based on the same L.T.B. curves for welded sections (§ 6.3.2.2). The proposed approach is based on an Ayrton-Perry format, and leads to a reduction factor χ_{LT} that is to be applied on the cross-section resistance, taking into account the penalty owing to member instability on the cross-sectional resistance. This χ_{LT} coefficient is calculated as follows:

5

$$\chi_{LT} = \chi_D = \frac{1}{\phi_{LT} + \sqrt{\phi_{LT}^2 - \overline{\lambda}_{LT}^2}} \leq 1.0 \qquad (1)$$

where the value to determine the reduction factor $\phi_{LT} = \phi_D = 0.5 \cdot \left[1 + \alpha_{LT} \cdot \left(\overline{\lambda}_{LT} - 0.2\right) + \overline{\lambda}_{LT}^2\right]$

fixes a length of 0.20 for the plastic plateau of the L.T.B. curves. The generalized imperfection factor α_{LT} varies from 0.21 to 0.76 according to the cross-section type. Since bridges girders are generally *plated* girders (i.e. *welded* beams), curves *c* (if section slenderness $h / b \leq 2$) and *d* (if $h / b \geq 2$) usually prevail.

In its current version, SIA263:2013 (SIA, 2013) Swiss standards for steel construction provides a similar expression to Eq. (1) but chooses a plastic plateau length of 0.4 and an imperfection factor $\alpha_D = \alpha_{LT} = 0.49$ for welded cross-sections.

3.2. F.E. parametric studies

Shell F.E. numerical models have been developed with the non-linear finite elements software FINELg (FINELg, 2003). Failure loads were obtained by means of Geometrically and Materially Non-linear with Imperfections Analyses (G.M.N.I.A.), while critical loads were calculated using Linear Bifurcation Analyses (L.B.A.). In the present study, S355 steel with a yield strength $f_y = 355$ *N/mm²* and a multilinear elastic-plastic material law as the one of Fig. 8 was used.
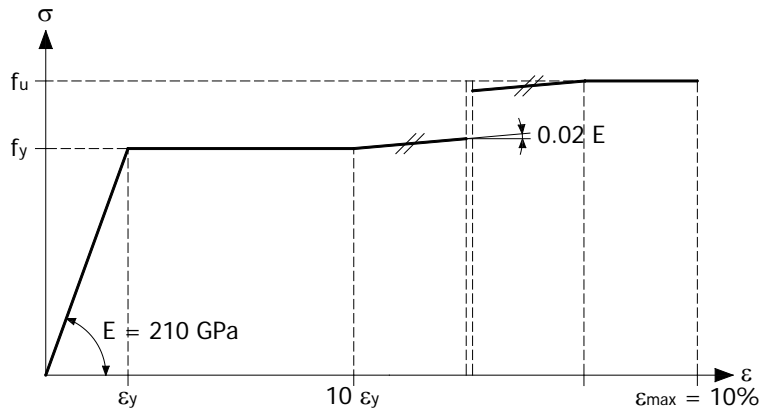

Figure 8: Material law considered in F.E. simulations

Two numerical shell models have been built so as to investigate L.T.B. in bridges:

- A *girder-type* model that considers a simple girder without any effect of cross-bracings. The loading consisted in a constant major-axis bending moment applied at the girder's extremities, and supports were defined to represent typical "fork" support conditions. This approach enables the evaluation of the influences of residual stresses or of initial imperfections on the resistance to L.T.B.;

- A *bridge-type* approach, where the model represents a "full" bridge with cross-bracings and lateral bracings, loaded with a uniformly distributed load. This model characterizes the various influences of the other parameters previously listed.

More precisely, the girder-type shell model accounts for geometrical imperfections modelled with an initial sinusoidal deformation (Fig. 9) with two deformation amplitudes: $\Delta = L / 1000$

and $\Delta = L / 3000$ where L is the girder span. Considering two deformation amplitudes enables to evaluate the sensitivity of the resistance to L.T.B. with the amplitude of the initial imperfection.
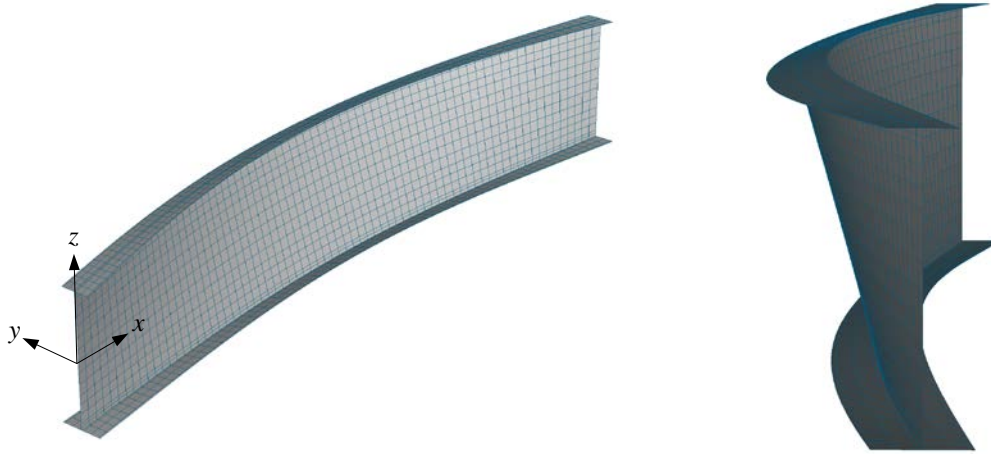

Figure 9: Initial imperfect geometry following a sinusoidal function (amplified 100x). (a) Axonometry. (b) View from the end of the girder

In order to determine the influence of residual stresses on the resistance to L.T.B. of a bridge girder, a case without residual stresses and three cases with different residual stresses models are considered for the numerical studies (Fig. 10). Fig. 10a follows the flame-cutting type residual stresses pattern from (ECCS, 1976). Fig. 10b follows the welding model from (ECCS, 1984). Fig. 10c follows the residual stresses experimental model proposed for flanges in Fig. 7b. For the web, the residual stresses pattern is based on the proposition from (Chacon, 2009), adapting the tensile width on the welded area to $h_w / 20$ with a stress value of $0.63\,f_y$.
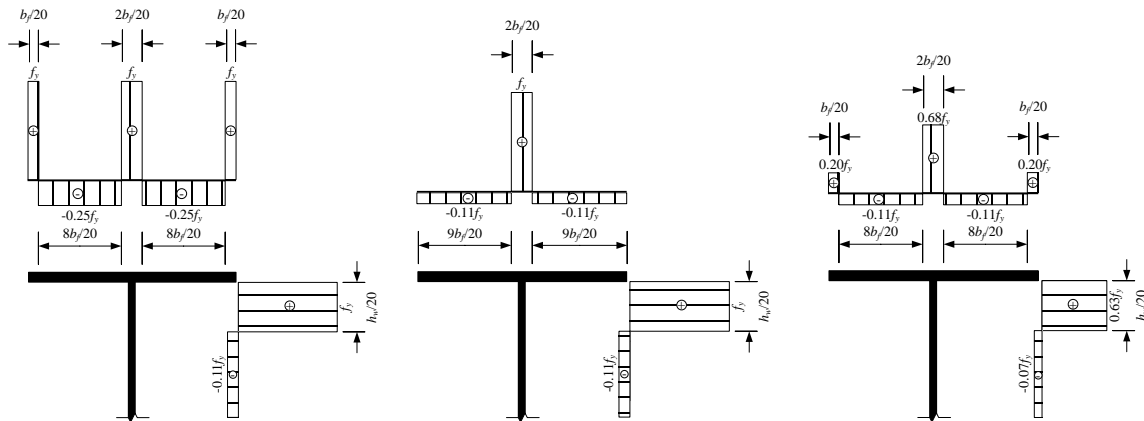

Figure 10: Residual stresses models considered for the numerical studies, $f_y = 355\ MPa$. (a) Model from (ECCS, 1976). (b) Model from (ECCS, 1984). (c) Model proposed in Fig. 7b

The bridge-type model considers a twin-girder bridge with a simple span L with different cross-bracing systems and an erection lateral bracing (Fig. 11). The spacing of the two girders was fixed to $6.0\ m$. The static system presents a fixed support and a support allowing lateral movement at one end, a free support and a support allowing longitudinal movement at the other end (Fig. 11). The uniform load applies at the center of the upper flanges.

The bridge-type F.E. models used both shell elements (girders, cross-bracings and stiffeners), and of bar elements for the truss girders. Failure loads were calculated using G.M.N.I.A. analyses, including as an initial geometrical imperfection the 1st critical mode shape of the L.B.A. calculation with an amplitude of $L / 1000$, where L is the span of the bridge. The residual stresses considered are the ones from Fig. 7b. Fig. 12 presents details on the support conditions and on different cross-bracing systems.
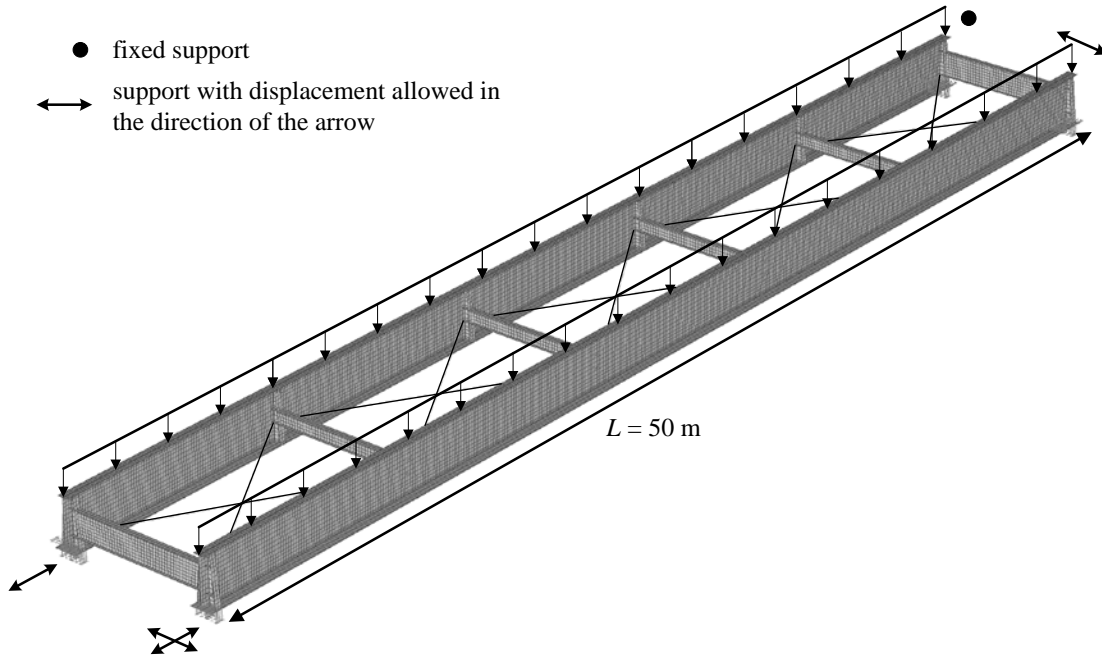

●   fixed support

↔   support with displacement allowed in the direction of the arrow

$L = 50$ m

Figure 11: Twin-girder model with a span $L = 50$ *m* and cross-bracings every 10.0 *m*
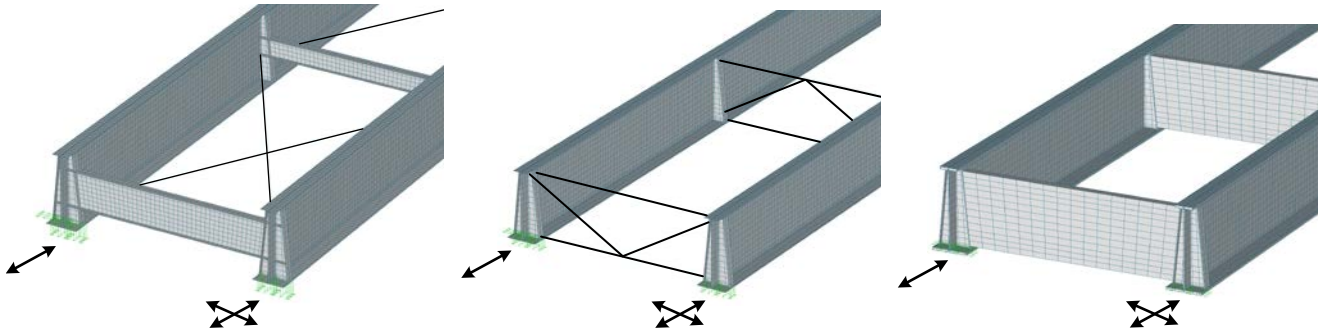

Figure 12: Details of the cross-bracings at girders' extremities. (a) Frame. (b) Truss. (c) Diaphragm

Two geometries of frame cross-bracing (Fig. 12a) have been considered in the present study; on the one hand, the cross-bracings on supports that are $h_f / 2$ high, and on the other hand, the ones located in span that are $h_f / 4$ high. The truss cross-bracings (Fig. 12b) are K-shaped and are modelled with square cross-sections truss elements. The diaphragms (Fig. 12c) are made of thick planar elements linking the upper and lower flanges. Further information on geometries are given in (Thiébaud, 2014). The parametric study focuses on two bridge girder cross-section geometries (Fig. 13).

8

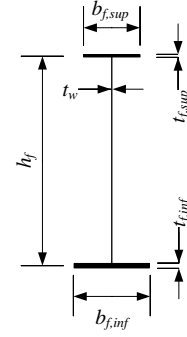| Type of section	h_f [m]	$b_{f,sup}$ [mm]	$t_{f,sup}$ [mm]	$b_{f,inf}$ [mm]	$t_{f,inf}$ [mm]	t_w [mm]
Wilwisheim (W)	3.2	800	40	1200	40	25
St-Pellegrino (SP)	2.0	450	20	650	40	14

Figure 13: Geometry of the considered cross-sections

Reporting F.E. reference results involved the following five steps:

- F.E. calculation of the L.T.B. critical moment M_{cr} through an L.B.A. analysis;

- Numerical calculation of the L.T.B. ultimate moment $M_{D,GMNIA}$ through the calculation of the failure load using a non-linear geometrical and material analysis;

- Analytical determination of the characteristic bending moment M_{Rk} that, in the case of bridge girders with a class 4 "slender" section, requires the calculation of the effective elastic section modulus related to the axis of the compressed flange $W_{eff,c}$;

- Determination of the relative slenderness $\bar{\lambda}_D = \bar{\lambda}_{LT} = \sqrt{\dfrac{M_{Rk}}{M_{cr}}}$;

- Calculation of the L.T.B. reduction factor $\chi_D = \chi_{LT} = \dfrac{M_{D,GMNIA}}{M_{Rk}}$.

By varying the lengths of the girders in the *girder-type* approach and the distance between cross-bracings in the *bridge-type* approach it is possible to obtain a series of $\lambda_D - \chi_D$ pairs, used as the F.E. reference for the comparison with the different L.T.B. curves as prescribed in European design codes.

4. Analysis of numerical results

4.1. Influence of residual stresses

Fig. 14 presents the influence of residual stresses on resistance to L.T.B. The results are obtained with the numerical model described in section 3.2 for the four following situations:

- Without residual stress (denoted as "W RS" on the following figures);

- Residual stresses taking into account the flame-cutting and welding according to Fig. 10c;

- Residual stresses taking into account the effect of welding only following the simplified model (ECCS, 1984) on Fig. 10b;

- Residual stress taking into account flame-cutting and welding according to the model (ECCS, 1976) on Fig. 10a.

The resistance to L.T.B. differences between the situations of residual stresses in Figs. 10c and 10b, as well as the Fig. 10b and without RS, are represented in Fig. 14 with labels Δ(c-b) and Δ(b-W RS), respectively.

For the studied cross-sections, the effect of the residual stresses on the resistance to L.T.B. is visible for a relative slenderness $\lambda_D < 1.4$. The effect is greatest for λ_D values ranging from 0.6 to 0.8, then stabilizes or even diminishes depending on the cross-section considered. Beyond the $\lambda_D = 1.4$ value, elastic L.T.B. behavior prevails.
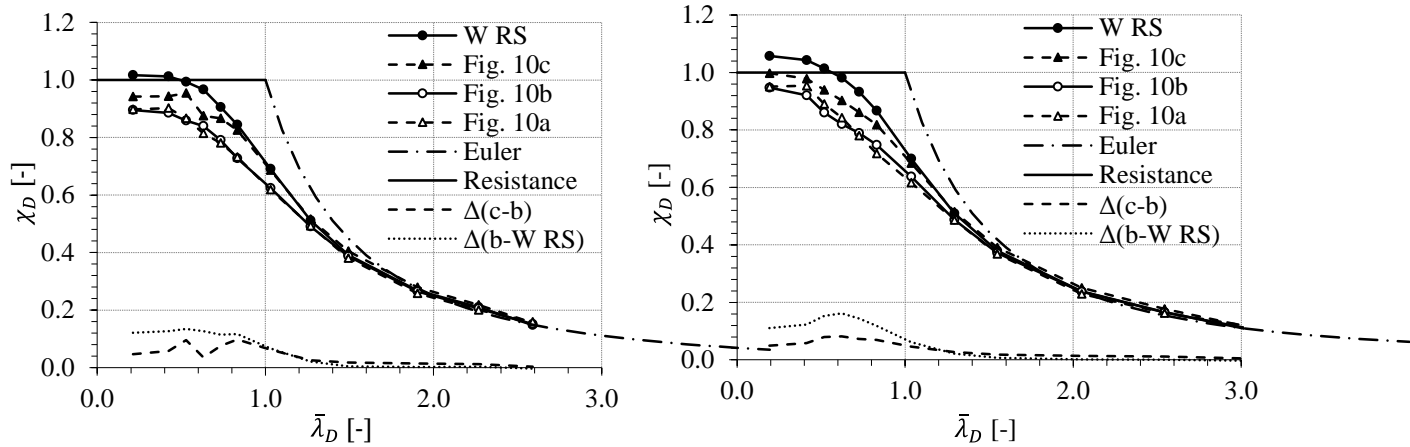

Figure 14: Influence of residual stresses. (a) St-Pellegrino-type section (SP). (b) Wilwisheim-type section (W)

Firstly, for both SP and W cross-sections (Figs. 14a and 14b), one immediately notices that the introduction of residual stresses decreases the resistance to L.T.B. as compared to an ideal girder without residual stresses. The differences given by the curves Δ(b-W RS) reach maximums of 13.5% for $\lambda_D = 0.53$ (Fig. 14a) and 16.1% for $\lambda_D = 0.62$ (Fig. 14b). These differences show that the effect of residual stresses on L.T.B. cannot be neglected.

The difference Δ(c-b) is also interesting since it shows the effect of the residual stresses due to flame-cutting as compared to a model of residual stresses developed for the welded profiles in buildings. The differences between those two situations reach maximums of 9.8% for $\lambda_D = 0.83$ (Fig. 14a) and of 8.2% for $\lambda_D = 0.62$ (Fig. 14b) in favor of the flame-cutting and welding model of residual stresses of Fig. 10c. It is therefore recommended to use the *flame-cutting and welding residual stresses model presented in Fig. 10c* within F.E. simulations of the failure load of steel slender plate girders in bridges, as this residual stresses model not only represents more precisely the fabrication process but also yields more economic results.

4.2. Influence of geometrical imperfections

Fig. 15 presents the influence of the amplitude of geometrical imperfections on the resistance to L.T.B. Case *L* / 1000, representing the manufacturing geometrical tolerances (SIA, 2013b), and case *L* / 3000, taking the values of geometrical imperfection measured in the study (Thiébaud, 2014), are compared.
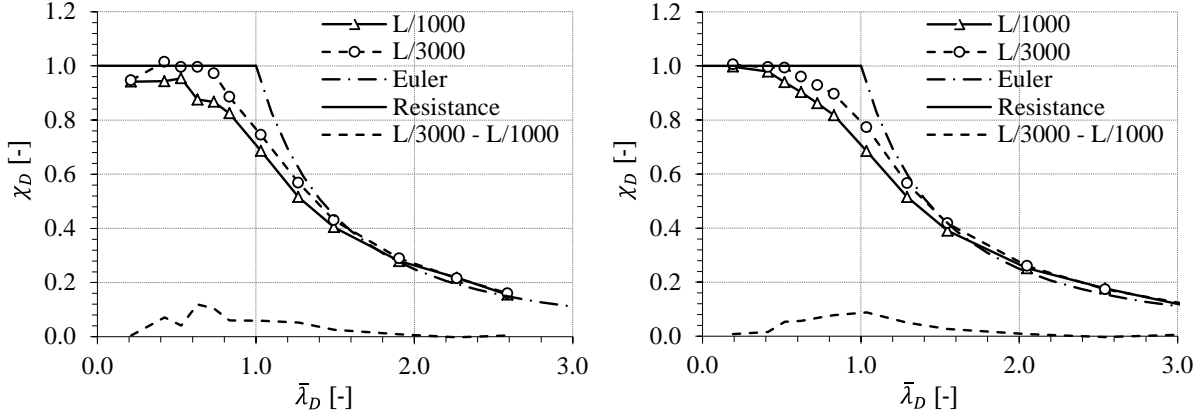
Figure 15: Influence of the amplitude of geometrical imperfections. (a) St-Pellegrino-type section (SP). (b) Wilwisheim-type section (W)

Figs. 15a and 15b obviously illustrate that when the amplitude of the imperfections decreases, the resistance increases (i.e. χ_D values are higher), even more so when the relative slenderness lies between 0.4 and 1.5. The resistance deviation, represented by the curve $L/3000 - L/1000$ in Fig. 15, shows maximum values of 11.9% for $\lambda_D = 0.63$ ("St-Pellegrino" geometry) and of 8.8% for $\lambda_D = 1.0$ ("Wilwisheim" geometry). Such results clearly indicate that the effect of the amplitude of geometrical imperfections may lead to significant differences. It follows that *the amplitude of $L/1000$ is recommended* for the calculation of the failure load of steel girders in bridges, both because it represents a reasonable value and for safety reasons. This value can also be shown to be safe-sided in comparison to experimental measurements (Thiébaud, 2014).

4.3. Influence of cross-bracings

Fig. 16 presents results relative to the influence of cross-bracings on the resistance to L.T.B. of a bridge with a 50 m span and a St-Pellegrino-type cross-section (SP50). The three types of cross-bracings (frame, truss and diaphragm) have a $7 - 8 - 10$ m spacing, in ascending order of relative slenderness in Fig. 16.
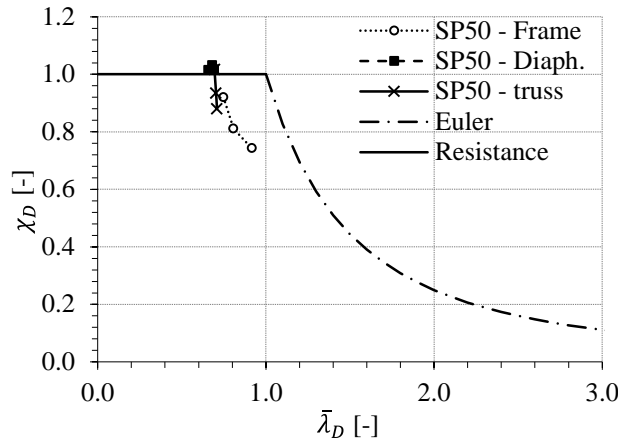

Figure 16: Influence of the cross-section types on the resistance to L.T.B.

As a first observation on the efficiency of different cross-bracing systems, Fig. 16 results clearly show that λ_D decreases as the cross-bracings rigidity increases, for an equal distance between

11

cross-bracings. As an example, one can note that, for a distance between cross-bracings of 10 m (corresponding to the point of each series with the greatest λ_D), the increase in resistance with respect to a *frame* cross-bracing is of 14% for a *truss* cross-bracing and of 27% for a *diaphragm* cross-bracing in the St-Pellegrino case.

Fig. 16 also shows that when the distance between cross-bracings decreases (i.e. when the number of lateral supports increases), the resistance to L.T.B. obviously increases. In the case of a frame cross-bracing, decreasing the distance between bracings from 10 m to 8 m then to 7 m increases the resistance by 7% and 17%, respectively. In the case of the truss cross-bracing, these increases are not as important since the cross-bracings are more rigid, but still show some 5% and 13% increases, respectively. As for the diaphragm cross-bracing, the full cross-sectional resistance ($\chi_D = 1.0$) is already reached with a distance between cross-bracings of 10 m.

Fig. 17 shows the shapes of the critical modes (on the left) chosen for the non-linear calculation of the SP cross-section and the L.T.B. failure shapes (on the right) associated with frame cross-bracings (Fig. 17a), truss cross-bracings (Fig. 17b) and diaphragm cross-bracings (Fig. 17c) with a distance between cross-bracings of 10 m.
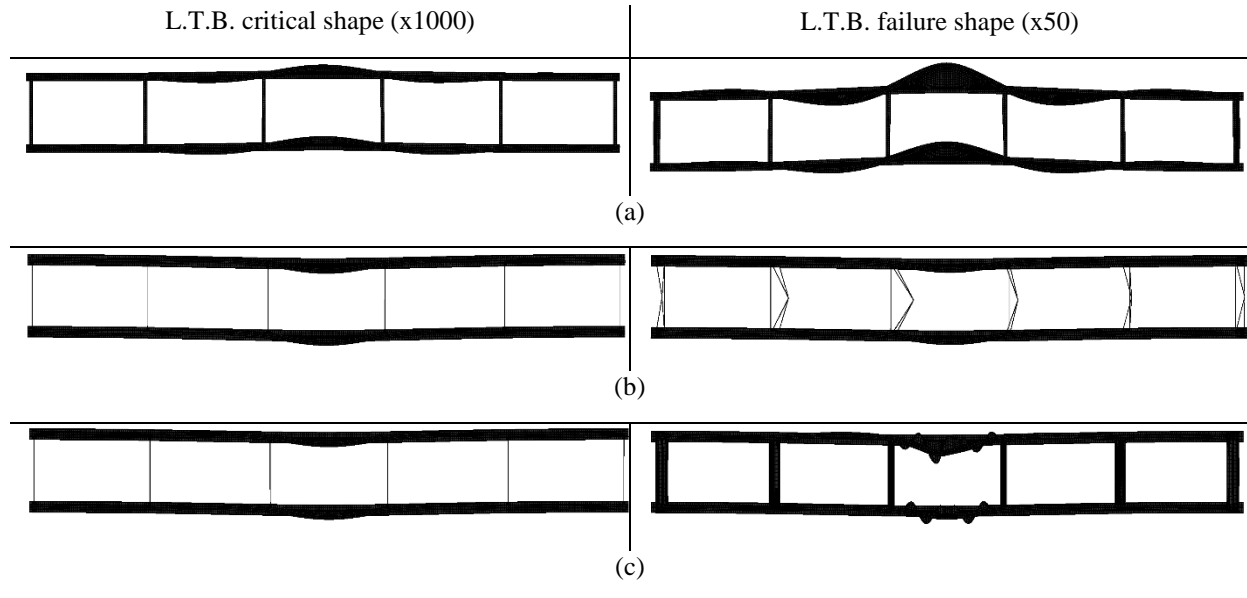
L.T.B. critical shape (x1000)	L.T.B. failure shape (x50)

(a)

(b)

(c)

Figure 17: Plan of critical shapes (on the left) and failure shape (on the right) for the SP cross-section. (a) SP50 – frame cross-bracing, $e = 10$ m, $\lambda_D = 0.917$; $\chi_D = 0.743$. (b) SP50 – truss cross-bracing, $e = 10$ m, $\lambda_D = 0.709$; $\chi_D = 0.879$. (c) SP50 – diaphragm cross-bracing, $e = 10$ m, $\lambda_D = 0.693$; $\chi_D = 1.017$

For all three types of cross-bracings, one naturally observes a good correspondence between the critical and failure modes; in addition, the maximum lateral displacement of both L.B.A. and G.M.N.I.A. computations is always seen to occur between two cross-bracings at mid-span, in the region of greatest major-axis bending moment, the adjacent spans being seen to somehow restrain L.T.B. of the weakest segment. By comparing the failure modes, it appears that for truss and diaphragm cross-bracings, the lateral deformations are mostly located in between cross-bracings, whereas for frame cross-bracings it also extends to the adjacent parts. Besides, the model with the diaphragm cross-bracings (Fig. 17c) shows for the failure shape that L.T.B. is coupled to local buckling in the web.

5. Analysis of code prescriptions for Lateral Torsional Buckling

This section analyses the obtained numerical results through comparisons with the analytical approaches available in the Swiss Standards SIA263:2013 (SIA, 2013) or the European Standards Eurocode EN1993-2:2006 (CEN, 2006), for both "girder-type" and "bridge-type" approaches so as to recommend a practical design method for the L.T.B. of bridge girders.

5.1. "Girder-type" model

From an analytical point of view, calculating λ_D for steel bridge girders requires the calculation of the L.T.B. critical stress σ_{cr} or the critical bending moment M_{cr}, which can be done using one of the two following methods:

1. The analytical procedure according to SIA263:2013 in § 5.6.2.3 leads to the following relative slenderness:

$$\bar{\lambda}_D = \sqrt{\frac{f_y}{\sigma_{crD}}} = \sqrt{\frac{f_y}{\pi^2 E \eta}} \sqrt{\frac{A_D}{I_D}} \cdot l_D \tag{2}$$

where A_D and I_D are respectively the area and weak axis second moment of area of a T section composed of the effective compression flange and of the half of the effective web in compression; η is a factor accounting for a non-constant distribution of bending along the girder ($\eta = 1$ for a constant bending moment). Eq. (2) shows that the relative slenderness is composed of a constant term $\sqrt{f_y / \pi^2 E \eta}$ and a term $\sqrt{A_D / I_D} \cdot l_D$ depending solely on the geometry and growing linearly with the unbraced length l_D;

2. In dividing the critical L.T.B. moment M_{cr} calculated with Djalaly's three factor formula[5] (Djalaly, 1974) by the effective elastic section modulus $W_{eff,c}$ of the class 4 cross-section. The relative slenderness is expressed by :

$$\bar{\lambda}_D = \sqrt{\frac{f_y}{\sigma_{crD}}} = \sqrt{\frac{f_y W_{eff,c}}{M_{cr}}} \tag{3}$$

Fig. 18 enables a comparison of the two analytical approaches as compared to the F.E. numerical results from section 4. The relative slenderness λ_D is represented as a function of the L.T.B. length l_D for the St-Pellegrino (SP – Fig. 18a) and Wilwisheim (W – Fig. 18b) sections. The relative slenderness values calculated numerically by the FINELg F.E. model are represented by the points SP – FinelG (Fig. 18a) and W – FinelG (Fig. 18b).

For the same girder geometries, the analytical expression in Eq. (2) leads to higher relative slenderness values up to 30% (case where $l_D = 30\ m$, Fig. 18a) as compared to the ones computed numerically by FINELg with the girder model. Assuming that the relative slenderness values calculated numerically are closer to reality, the analytical expression SIA263:2013 – § 5.6.2.3 leads to safe-sided resistance predictions, since higher λ_D values are associated to lower χ_D ones.

Oppositely, the three factors analytical expression (Djalaly, 1974) used for the calculation of l_D as in Eq. (3) shows an excellent correspondence with the numerically calculated ones (Figs. 18a

---

[5] Space is missing here to give full details on the Djalaly's method. The interested reader may usefully refer to (Djalaly, 1974).

and 18b) – non-linear dependence of λ_D with l_D is indeed taken into account by Eq. (3). Thus, keeping the slenderness values calculated numerically as references, the analytical expression (Djalaly, 1974) enables one to place λ_D with increased accuracy on the $\chi_D - \lambda_D$ diagram, generally leading to a gain on the evaluation of the resistance to L.T.B.
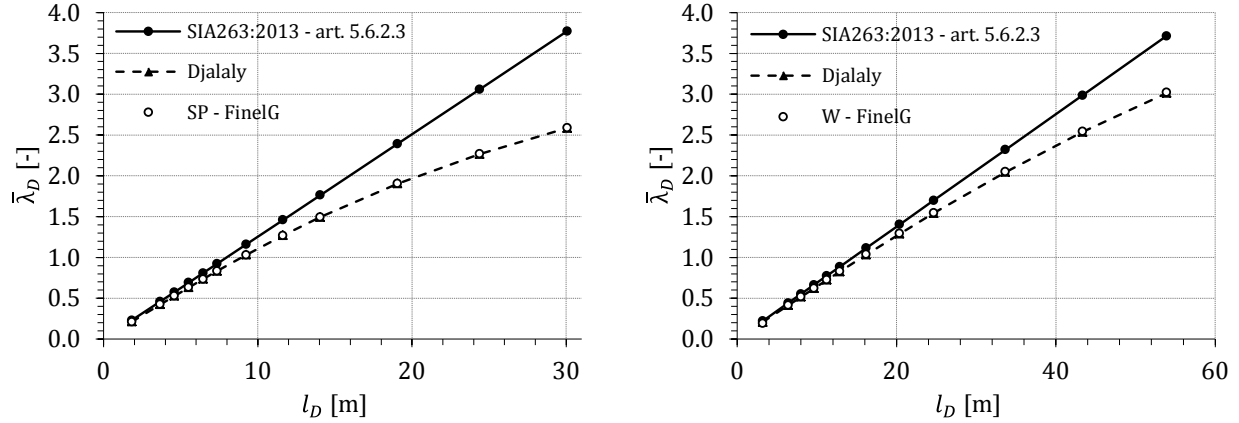

Figure 18: Comparison of the calculation of the relative slenderness as a function of the unbraced length l_D. (a) St-Pellegrino-type section (SP). (b) Wilwisheim-type section (W)
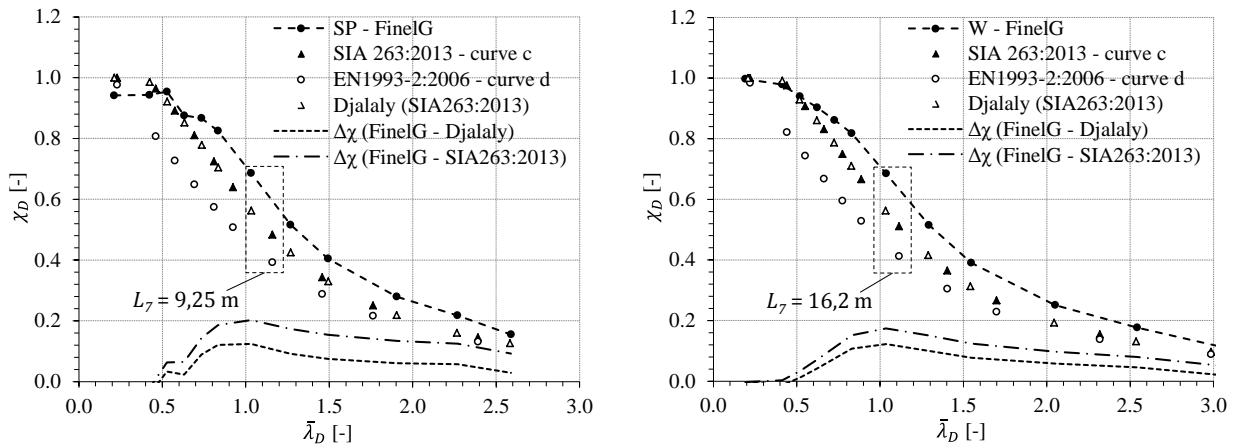

Figure 19: Numerical and analytical comparison of χ_D with the girder type approach. (a) St-Pellegrino-type section (SP). (b) Wilwisheim-type section (W)

Fig. 19 compares the analytical and numerical approaches of the reduction factor χ_D for the St-Pellegrino (Fig. 19a) and Wilwisheim (Fig .19b) cross-sections. Analytically, the relative slenderness values λ_D are determined as presented in Fig. 18 and detailed previously. The reduction factor χ_D is determined analytically with buckling curve c for the SIA263:2013 standard and curve d for EN1993-2:2006 European standards. Besides, the curves $\Delta\chi$ represent the following resistance differences:

1. $\Delta\chi$ (FinelG – Djalaly) represents the deviation in resistance to L.T.B. between the FINELg numerical simulations and the SIA263:2013 curve c for a relative slenderness calculated using the method recommended by Djalaly in (Djalaly, 1974);

14

2. $\Delta\chi$ (FinelG – SIA263:2013) represents the deviation in resistance to L.T.B. between the FINELg numerical simulations and SIA263:2013 curve c for a relative slenderness calculated using the SIA263:2013 – § 5.6.2.3 method.

For the SP section (Fig. 19a), the analytical results (SIA263:2013 – curve c, EN1993-2:2006 – curve d and Djalaly) remain below the numerical results (SP – FinelG) for a relative slenderness λ_D bigger than 0.5. For smaller relative slenderness values ($\lambda_D = 0.2$ and 0.4), the F.E.-computed resistances are below the values from curve c from SIA263:2013. These values correspond to girders with lengths $L_1 = 1.83\,m$ and $L_2 = 3.67\,m$ for a girder height of $h_f = 2.0\,m$. The corresponding girder slenderness values (L/h) are 0.9 and 1.8, values that are not representative of bridge girders and triggers other structural behaviors than L.T.B. (e.g. concentrated bearing stresses, local buckling…). Therefore, the relevance of such results shall be left aside in the development of an improved design method against L.T.B.

Cross-section SP (Fig. 19a) shows a difference in resistance $\Delta\chi$ (FinelG – Djalaly) reaching a maximum of 12% for a relative slenderness $\lambda_D = 1.0$ corresponding to a girder length $L_7 = 9.25\,m$. For this same girder, however with λ_D calculated with SIA263:2013 – § 5.6.2.3, the deviation of resistance $\Delta\chi$ (FinelG – SIA263:2013) grows again, reaching 0.20 (20%). These differences bring out the existing margin between the numerical simulations and the SIA263:2013 standard – curve c.

For section W (Fig. 19b) the analytical calculations (SIA263:2013 – curve c, EN1993-2:2006 – curve d and Djalaly) remain smaller or equal to their numerical counterparts (W – FinelG) for all the considered reduced slenderness values λ_D – i.e. safe-sided. For the girder whose length is $L_7 = 16.2\,m$, the maximum resistance deviations are similar to SP and reaches 0.12 (12%) for $\Delta\chi$ (FinelG – Djalaly) and 0.17 (17%) for $\Delta\chi$ (FinelG – SIA263:2013) for a relative slenderness of $\lambda_D = 1.0$ (Fig. 19b).

Therefore, for both SP and W geometries, a design approach characterized by i) the calculation of λ_D by means of Eq. (3) and Djajaly's three factor formula, and ii) by the use of buckling curve c shall be recommended.

5.2. "Bridge-type" model

Fig. 20 presents the relative slenderness values λ_D calculated analytically with Eq. (2) and numerically as a function of the distance e between cross-bracings. The relative slenderness values calculated analytically take into account the in-plane cross-bracings' rigidities in calculating the unbraced length l_D according to clause 5.5.3.1 of SIA263:2013. The results are valid for frame cross-bracings every 5 to $10\,m$ and for St-Pellegrino (SP – Fig. 20a) and Wilwisheim (W – Fig. 20b) cross-sections with a constant distributed transverse load applied to the upper flange.
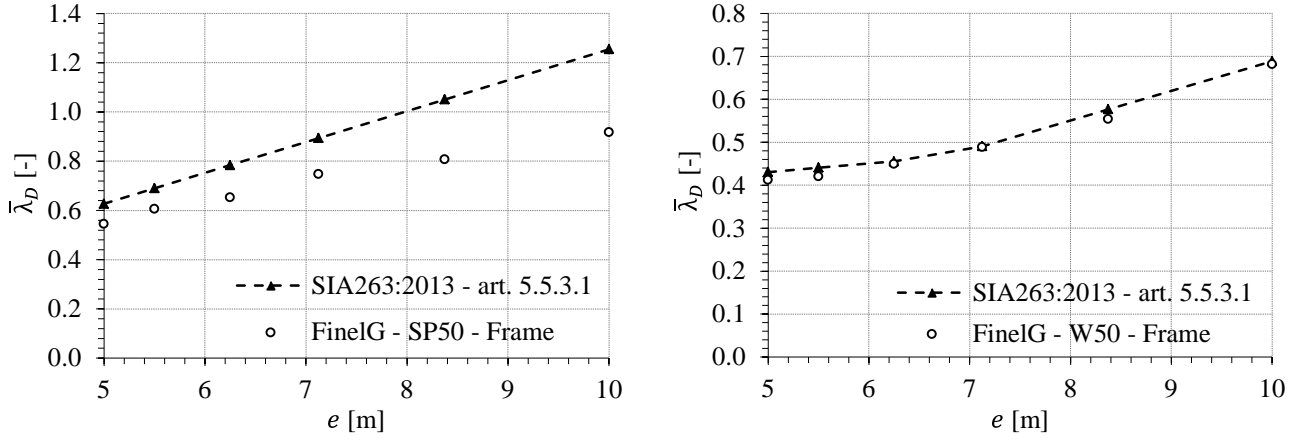
Figure 20: Comparison of the calculation of the relative slenderness as a function of the cross-bracings' spacing e. (a) St-Pellegrino-type section (SP). (b) Wilwisheim-type section (W)
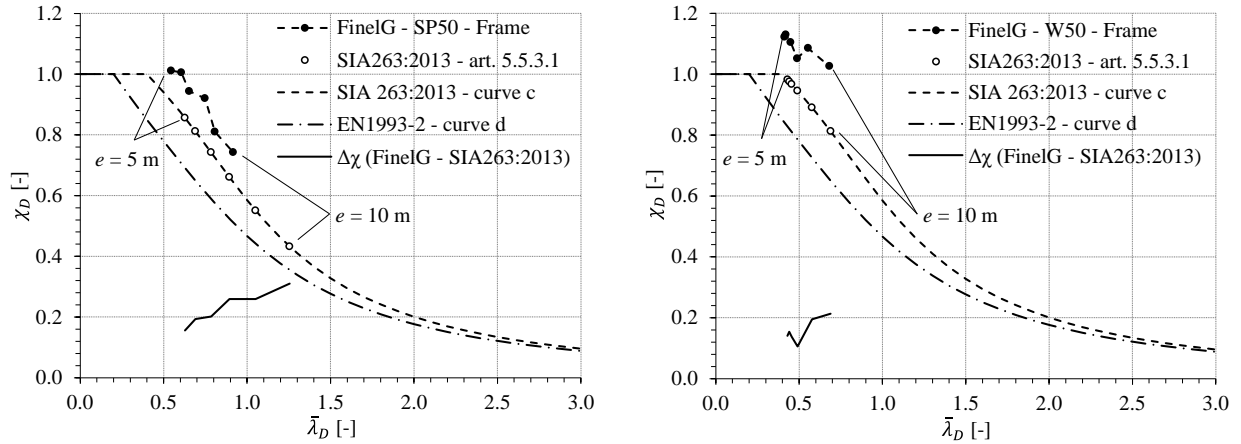

Figure 21: Comparison of analytical and numerical results of the χ_D calculation for the bridge type approach. (a) St-Pellegrino-type section (SP). (b) Wilwisheim-type section (W)

For bridges with a St-Pellegrino section (Fig. 20a), the results show that the analytical approach (SIA263:2013 – § 5.5.3.1) tends to overestimate the numerical prediction (FinelG – SP50 – Frame) for λ_D values. This tendency remains safe since the reduction factor χ_D decreases as λ_D increases. The deviation between the analytical and numerical approaches is also seen to grow when e increases. For example, for a distance between cross-bracings $e = 5\ m$, λ_D is overestimated by 15%, while for $e = 10\ m$ it is overestimated by 36%.

For bridges with a Wilwisheim section (Fig. 20b), the results show that the analytical approach (SIA263:2013 – § 5.5.3.1) much better evaluates the relative slenderness as compared to the reference numerical calculations (FinelG – W50 – Frame). The deviations in λ_D between the analytical and the numerical approaches are very small, and reach a maximum of 5% for a distance between cross-bracings $e = 5.5\ m$.

Fig. 21 compares the analytical and numerical approaches for the determination of factor χ_D for St-Pellegrino (Fig. 21a) and Wilwisheim (Fig. 21b) cross-sections. The six dots on Figs. 21a and

21b correspond, for increasing λ_D values, to distances between cross-bracings of 5 – 5.5 – 6.25 – 7.125 – 8.375 – 10 *m*, respectively.

For bridges with a St-Pellegrino section (Fig. 21a), the numerical results (FinelG – SP50 – Frame) show that they are above the SIA263:2013 reduction curve *c* with an appreciable safety margin around 7 to 8%. When the numerical results are compared to the analytical ones (SIA263:2013 – § 5.5.3.1), deviations in the reduction factors χ_D, represented by the curve $\Delta\chi$ in Fig. 21a, increase when λ_D increases. This is consecutive to overestimations of λ_D values by SIA263:2013 –§ 5.5.3.1 (Fig. 20a) analytical calculation method which shifts λ_D to the right side following curve *c* of SIA263:2013. For example, $\Delta\chi$ spans from 0.15 (15%) for a distance between cross-bracings of *e* = 5 *m* to a maximum of 0.31 (31%) for *e* = 10 *m* (Fig. 21a).

For bridges with a Wilwisheim section (Fig. 21b), the numerical results (FinelG – W50 – Frame) show, as for the SP section, that they are well above the reduction curve *c* of SIA263:2013. The safety margin is comfortable since it reaches values up to 20% for a distance between cross-bracings of *e* = 10 *m*. However, when the numerical results are compared to their analytical counterparts (SIA263:2013 – § 5.5.3.1), the increased accuracy in the relative slenderness calculation (Fig. 20b) enables a better "positioning" of the analytical λ_D as compared to the numerical one. This decreases the difference $\Delta\chi$ in reduction factors as compared to the SP section, as is shown on Fig. 21b. For example, the reserve of resistance $\Delta\chi$ goes from 0.14 (14%) for a distance between cross-bracings of *e* = 5 *m* to 0.21 (21%) for *e* = 10 *m* (Fig. 21b).

The same conclusions as for the "girder-type" approach shall apply here to the "bridge-type" approach, i.e. i) the calculation of λ_D by means of Eq. (3) and Djajaly's three factor formula, and ii) the use of buckling curve *c* can safely be recommended.

5.3. Recommendation of a buckling curve

On Fig. 22, a total of 186 points represents the whole set of numerical results exposed previously alongside with the results of a M.Sc. project (Torriani, 2014). On the same graph, curves *b* and *c* from SIA263:2013 standard and curve *d* from Eurocode 1993-2:2006 are represented.
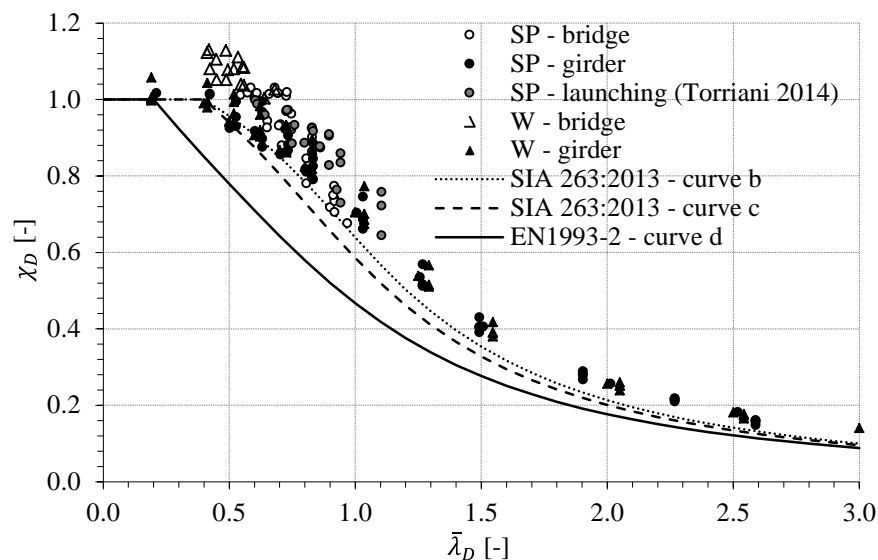

Figure 22: Representation of all numerical results obtained for the L.T.B. of bridge girders

In Fig. 22, the differences in L.T.B. resistance $\Delta\chi_D$ between the reduction factors calculated numerically ($\chi_{num.}$) using the girder type and FINELg bridge type approaches to FINELg and standards' reduction curves ($\chi_{num.}$) are represented in Figs. 23. The differences in resistance for SIA263:2013 curve b are given in Fig. 23a, those with SIA263:2013 curve c in Fig. 23b and those from EN1993-2:2006 curve d in Fig. 23c.

The SIA263:2013 reduction curve b shows differences in resistance (Fig. 23a) reaching a maximum of 0.20 (20%), with an average $\Delta\chi_D$ equal to 0.07 and a standard deviation equal to 0.05. The number of numerical results on the unsafe side $\Delta\chi_D < 0$ is 11 out of 186 and is relative to λ_D values lower than 1.0 for the *girder* and *bridge*-type approaches, as shown in Fig. 22.

The differences increase when compared to SIA263:2013 curve c (Fig. 23b), the maximum values reaching 0.25 (25%). The average $\Delta\chi_D$ lies around 0.10 with a standard deviation of 0.06. The number of numerical results on the unsafe side decreases to 4 out of 186 and concerns relative slenderness values λ_D smaller than 0.60 for the girder type approach only (Fig. 22). No numerical result from the bridge type approach is on the unsafe side of curve c.

EN1993-2:2006 reduction curve d shows important differences in resistance (Fig. 23c) up to 0.38 (38%) with an average $\Delta\chi_D$ equal to 0.20 and a standard deviation equal to 0.10. No numerical value is on the unsafe side of curve d.
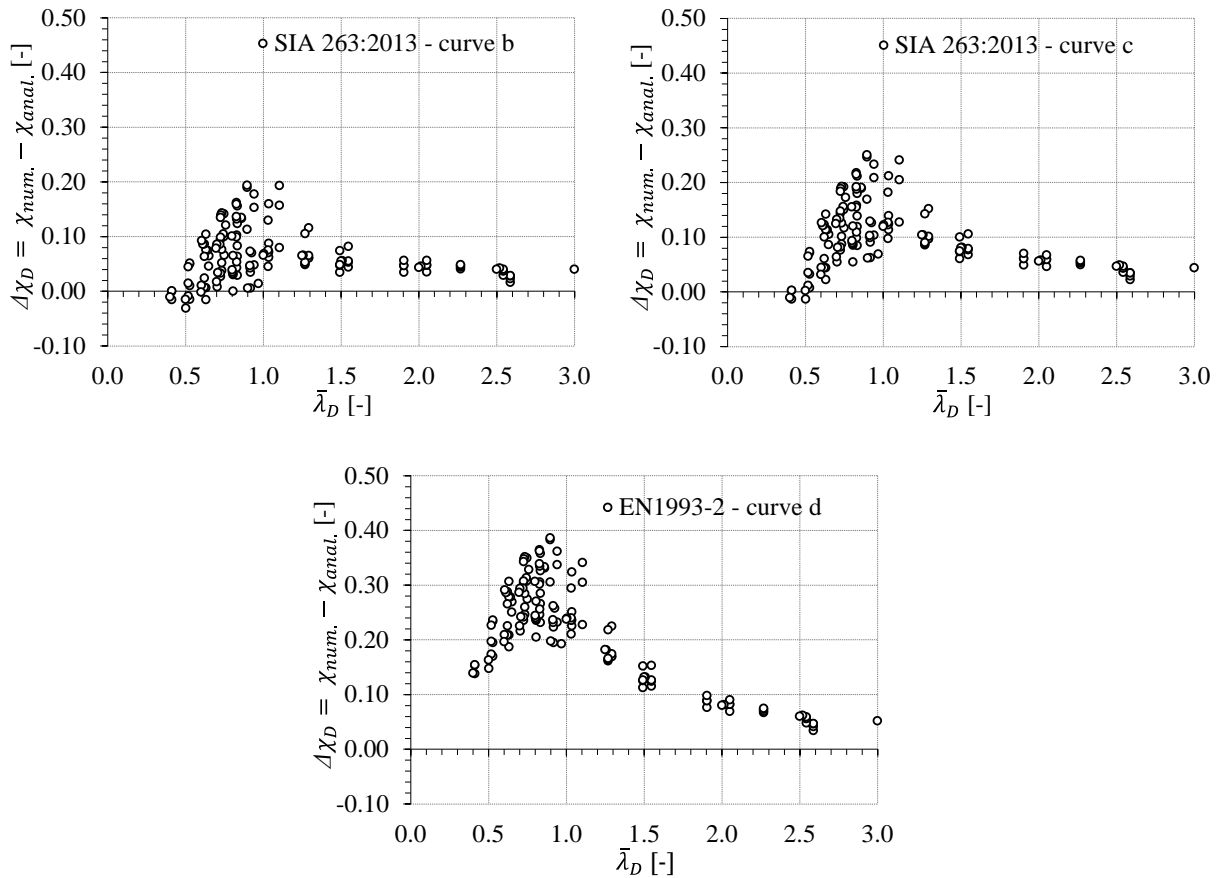

Figure 23 Differences on χ_D between the numerical results and the L.T.B. curves. (a) SIA263:2013 curve b case. (b) SIA263:2013 curve c case. (c) EN1993-2:2006 curve d case.

6. Conclusions

The present paper was dedicated to the L.T.B. behavior and response of welded bridge girders. In particular, the distribution of characteristic residual stresses within the cross-section was investigated experimentally. These studies have enabled the definition of a residual stresses pattern suited to steel bridge girders that properly reflects the manufacturing stages of flame-cutting and welding.

Then, the paper has investigated the various influences on the resistance to L.T.B. of residual stresses, geometrical imperfections and cross-bracing systems, both on isolated girders and on a twin-girder steel bridge for the latter. Numerical and analytical studies allowed validating a verification method adapted to bridge steel girders, and its key features shall be summarized as follows:

- In the case of an isolated steel bridge girder without lateral bracing, an analytical determination of the L.T.B. relative slenderness λ_D is possible with a high accuracy through the three factors expression giving the critical bending moment value M_{cr} as recommended by Djalay (cf. (Djalaly, 1974));

- For an isolated steel bridge girder elastically supported by cross-bracings (typically during the erection phase), the calculation of the relative slenderness λ_D may be done safely through a simplified formula mainly involving the unbraced length l_D;

- SIA263:2013 and EN1993-2:2006 buckling curve c leads to safe estimates of the reduction factor χ_D, leading to higher L.T.B. resistances than presently prescribed in these codes (curve d is recommended in EN1993-2:2006). Deeper investigations (e.g. reliability analyses) may be found in (Thiébaud, 2014).

Acknowledgements

References

CEN (2006). "Eurocode 3 – Calcul des structures en acier – Partie 2: Ponts métalliques."

Chacón R, Mirambell E, Real E. (2009). "Influence of designer-assumed initial conditions on the numerical modelling of steel plate girders subjected to patch loading." *Thin-Walled Structures; 47:391–402. doi:10.1016/j.tws.2008.09.001.*

Djalaly H. (1974). "Calcul de la résistance ultime au déversement. " *Construction Métallique 58–77.*

ECCS (1976). "Manual for Stability of Steel Structures (2nd ed.)." *ECCS Committee 8 – Stability.*

ECCS (1984). "Ultimate limit state calculation of sway frames with rigid joints." *ECCS Committee 8 – Stability.*

FINELg (2003). "Programme d'élément finis non-linéaire FINELg." *Université de Liège, Bureau d'Etudes Greisch.*

Gozzi J. (2007). "Patch loading resistance of plated girders: ultimate and serviceability limit state." *Luleå University of Technology.*

SIA (2013). "Constructions en acier."

SIA (2013b). "Constructions en acier – Spécifications complémentaires."

Tebedge N., Alpsten G., Tall L. (1973). "Residual-stress measurement by the sectioning method." *Experimental Mechanics;13:88–96.*

Thiébaud R. (2014). "Résistance au déversement des poutres métalliques de pont." *École polytechnique fédérale de Lausanne EPFL.*

Torriani R. (2014). "Etude de la résistance au déversement d'une poutre métallique de pont lors du lancement. " *École polytechnique fédérale de Lausanne EPFL.*